

Article

Synthesis, Characterization, and Antibacterial Activity of Silver Nanoparticles Supported on Bovine Bone Powder Using *Heterotheca inuloides*: An In Vitro Study

Sergio Arturo Gama-Lara ^{1,*} , Alfredo Rafael Vilchis-Néstor ² , Adriana Moreno-Rodríguez ³ ,
Liliana Argueta-Figueroa ⁴ , Marco Antonio Zamora-Antuñano ⁵  and Martha Stephanie Pérez-Mendoza ²

- ¹ Engineering Department, CIIDETEC-Toluca, Universidad del Valle de México, Toluca 52164, Mexico
² Centro Conjunto de Investigación en Química Sustentable UAEM-UNAM, Carretera Toluca-Atlaconulco Km 14.5, San Cayetano, Toluca 50200, Mexico; arvilchisn@uaemex.mx (A.R.V.-N.); steph.pm@yahoo.com (M.S.P.-M.)
³ Facultad de Ciencias Químicas, Universidad Autónoma Benito Juárez de Oaxaca, Av. Universidad s/n, Ex-Hacienda de Cinco Señores, Oaxaca 68120, Mexico; arimor10@hotmail.com
⁴ Conahcyt-National Technological Institute of Mexico/Toluca Technological Institute, Av. Tecnológico s/n, Colonia Agrícola Bellavista, Metepec 52149, Mexico; l_argueta_figueroa@hotmail.com
⁵ Engineering Department, CIIDETEC-Querétaro, Universidad del Valle de México, Querétaro 76230, Mexico; marco.zamora@uvmnet.edu
* Correspondence: gamaliel350@gmail.com; Tel.: +52-7221694529

Abstract: This paper reports on the biosynthesis, characterization, as well as the bactericide and cytotoxic properties of silver nanoparticles supported on bovine bone powder (Ag-NPs/BBP). The silver nanoparticles were obtained through the bioreduction of AgNO₃, using an infusion of *Heterotheca inuloides* leaves and flowers as a reducing agent and bovine bone powder as a support. The ratio of Ag-NPs/bovine bone powder was set as 1:10. The characterization was performed with SEM-EDS, XRD, UV-Vis, and TEM, which showed the formation of nanoparticles with an average size of 22.6 ± 10.8 nm and a quasi-spherical Ag-NPs morphology supported on the BBP surface. The nanocomposite exhibited a band gap of 2.19 eV. The minimal inhibitory concentration and the minimal bactericidal concentration against *S. aureus*, *E. coli*, and *S. epidermidis* were determined for each strain. In addition, the cytotoxic evaluation of the Ag-NPs/BBP on J774.2 mouse macrophage cells was performed. The Ag-NPs/BBP exhibited a bactericide effect on the strains studied, and the cytotoxicity had a dose-dependent behavior on the cells studied. Therefore, it was found that the ecofriendly synthesized Ag-NPs supported on bovine bone powder resulted in an effective bactericidal system against the strains studied, without significant cytotoxicity.

Keywords: Ag nanoparticles; *Heterotheca inuloides*; hydroxyapatite; bionanocomposite; bactericide effect; minimum inhibitory concentration



Citation: Gama-Lara, S.A.; Vilchis-Néstor, A.R.; Moreno-Rodríguez, A.; Argueta-Figueroa, L.; Zamora-Antuñano, M.A.; Pérez-Mendoza, M.S. Synthesis, Characterization, and Antibacterial Activity of Silver Nanoparticles Supported on Bovine Bone Powder Using *Heterotheca inuloides*: An In Vitro Study. *J. Compos. Sci.* **2024**, *8*, 142. <https://doi.org/10.3390/jcs8040142>

Academic Editors: Thanasis Triantafyllou and Francesco Tornabene

Received: 1 March 2024

Revised: 26 March 2024

Accepted: 7 April 2024

Published: 11 April 2024



Copyright: © 2024 by the authors. Licensee MDPI, Basel, Switzerland. This article is an open access article distributed under the terms and conditions of the Creative Commons Attribution (CC BY) license (<https://creativecommons.org/licenses/by/4.0/>).

1. Introduction

Over the last few decades, nanostructured systems have received a great amount of attention from several research groups [1].

For example, silver nanoparticles (Ag-NPs) have been used for the prevention and treatment of many oral diseases; due to that, Ag-NPs have been incorporated into different dental biomaterials as restorations, coatings, cavity linings, adhesives, varnishes, toothpastes, mouthwashes, among others, some of which are commercially available [2]. One of the most important properties of Ag-NPs are their bactericidal activity. At present, bionanotechnology may contribute to the design of new antimicrobial materials [3]. Ag-NPs are a good alternative to antimicrobial drugs or disinfection compounds. Furthermore, Ag-NPs synthesized by plant extracts could exhibit better properties in comparison with Ag-NPs synthesized by a conventional chemical reduction, because the active components of plants

may contribute to the antimicrobial effect of the NPs. For instance, Ag-NPs synthesized using an *Orchidantha chinensis* extract showed inhibitory effects on *S. aureus*, *P. aeruginosa*, and *E. coli* [4]; whereas, Ag-NPs synthesized with *Setaria verticillata* have been tested for the treatment of breast cancer [5], and Ag-NPs synthesized using a *Cynara cardunculus* extract exhibited bactericide properties against *E. coli* and *S. aureus* [6]. Ag-NPs synthesized using an *Acorus calamus* extract showed great bactericide activity against *Bacillus subtilis*, *Bacillus cereus*, and *S. aureus* [7]. Likewise, Ag-NPs obtained using a banana peel extract showed bactericide properties against *B. subtilis*, *E. coli*, and *S. aureus* [8].

In addition to this, it is important that metallic nanoparticles are supported on a material that possesses great electromagnetic affinity and prevents the loss of the NPs during the chemical reaction and allows them to be recovered at the end of use. It has been reported that Ni/Pd NPs have been supported on multi-walled carbon nanotubes [9], palladium on graphene [10] and graphene oxide [11], gold on TiO₂ and Al₂O₃ [12], and on silica [13], among others. Several authors have chosen to use a natural support, due to this these materials are ecofriendly, cheaper, and renewable, like cellulose [14], core shell [15], *Agave lechuguilla* and silk [16], and cotton fibers [17], among others. For this research, bovine bone powder (BBP) was used, which is constituted mainly by hydroxyapatite Ca₅(PO₄)₃(OH) and collagen [18], a microporous material with a high electronic density provided by OH⁻ and PO₄³⁻ functional groups [19]; these groups have the function of attracting and anchoring metallic silver ions to the surface of the support. Chicken bone has been used to support silver nanoparticles, using dimethylformamide (DMF) and poly(vinyl acetate) (PVA) as reducing and stabilizing agents, and an aqueous extract of Indian curry leaf (*Murraya koenigii*) with bactericidal properties was used [20,21].

In order to avoid toxic chemical waste during the fabrication of nanoparticles, the green synthesis of Ag-NPs has been carried out by different research groups, mainly using microorganisms or plant extracts. Polyphenols are the main constituents of different types of tea infusions and are responsible for their antimicrobial and antioxidant properties [22]. For green synthesis, polyphenols act to reduce the precursor salt. This synthesis route has been employed by many authors using tannins [23], *Ocimum sanctum* [24], *Dracocephalum moldavica* [25], *Citrus sinensis* [26], *Achillea biebersteinii* [27], *Origanum vulgare* [28], and *Commelina nudiflora* [1], among others. *Heterotheca inuloides* is a plant that shows great antimicrobial, anti-inflammatory, regenerative, and antioxidant properties. These properties are attributable to the large amount of polyphenolic compounds [29–31]. Due to that, *Heterotheca inuloides* has been used in traditional medicine and the pharmaceutical industry [29–32]. Aqueous extracts of *Heterotheca inuloides* have demonstrated high efficiency in the synthesis of noble metal nanoparticles, as Ag [16,33] and Pt [34] NPs. However, not only is the formation of nanoparticles expected, but also an improvement in the antimicrobial capacity attributable to the properties of the extract and the synergistic effects with the silver nanoparticles. This study aimed to report on the ecofriendly synthesis of Ag-NPs, using *Heterotheca inuloides* as a bioreducer, supported on bovine bone powder, in order to obtain a nanocomposite with increased antimicrobial activity against *S. aureus*, *E. coli*, and *S. epidermidis*, and a low level of cytotoxicity in contact with mouse macrophage cells.

2. Materials and Methods

2.1. Synthesis

In order to use a sustainable support, the femur bone of a bovine was chosen. The first step to prepare the support was to clean it, then it was cut into small pieces, powdered and, finally, sieved with a 150 mesh.

In order to obtain an environmentally friendly system, without toxic chemical waste, with a biodegradable, disposable, easily treated support, using the optimal amount of silver and an application focused on reducing diseases, Ag-NPs were synthesized on BBP using an infusion of *Heterotheca inuloides* as a reducing agent. It has been reported that the reductive properties of *Heterotheca inuloides* are mainly attributed to the reductive potential of the polyphenol (kaempferol, quercetin, and luteolin, among others), phenol (guaiacol, catechin,

and ellagic acid, among others), and sesquiterpene compounds (7-hydroxycadalene, cadalene, cadalen-15-oic acid, and dicadalenol, among others) present in the leaves and flowers of the plant [16,29,34,35].

The method that we used for the synthesis of the Ag-NPs was based on green chemistry principles and biotechnology. AgNO₃ was used as a precursor salt, and an infusion of *Heterotheca inuloides* leaves and flowers was used as a reducing agent. Two solutions were prepared: first, 100 mL of 0.001 M AgNO₃ (Meyer, Mexico City, Mexico) in deionized water. For the second solution, 1.5 g of *Heterotheca inuloides* leaves and flowers was put into 250 mL of boiling water for 1 h; the pH was not adjusted at any time. To synthesize the Ag/BBP bionanocomposite with a 1:10 ratio, 1 g of bovine bone powder was immersed in 92 mL of AgNO₃ solution for 30 s and then filtered; afterwards, the reduction of the Ag⁺¹ ions was carried out by adding 184 mL of the second solution. The mixture was kept under stirring for 1 h and then filtered. Finally, the powder was dried overnight at room temperature and atmospheric pressure. The experiments were performed as described in a previous work carried out by our research team [36].

2.2. Characterization

The crystal structure analysis for the composite was carried out using the powder X-ray diffraction (XRD) technique, performed in a Bruker *D8 Advance* diffractometer with Bragg–Brentano geometry, using Cu K α radiation, and a *LynxEye* detector. Optical characterization was achieved using the UV–Vis spectroscopy technique, in an Ocean Optics DT-1000 CE UV/vis spectrophotometer. For morphology analysis, the scanning electron microscopy (SEM) technique was performed. The samples were analyzed in JEOL JSM-6510LV equipment, coupled with an energy dispersive X-ray spectroscopy (EDS) detector from Oxford for the elemental analysis. In order to analyze the size and shape of the Ag-NPs, electronic transmission microscopy observations (TEM) were also performed; in this case, the samples were suspended in 2-propanol and then ultrasonically dispersed for 5 h at room temperature. A drop of this suspension was then placed on a Cu grid coated with a holey carbon film. The studies were carried out using a JEOL JEM-2100 microscope, operated at 200 kV with an LaB₆ filament. An Agilent Cary 630 FTIR instrument, with an ATR sampling module, with the serial number MY2149CUo5, was used for the Fourier transform infrared spectroscopy. The characterization was performed as described in a previous work carried out by our research team [36].

2.3. Biological Properties

Antibacterial evaluation. The bacterial strains used in this study were obtained from the stock culture collection of the Universidad Autónoma Benito Juárez de Oaxaca. The experiments were performed as described in a previous work carried out by our research team [37]. The antimicrobial activity of the Ag-NPs/BBP was tested against *Staphylococcus aureus* (*S. aureus*), *Escherichia coli* (*E. coli*), and *Staphylococcus epidermidis* (*S. epidermidis*). The broth method was followed in order to determine the minimal inhibitory concentration (MIC) and the minimal bactericidal concentration (MBC). Specifically, 100 μ L of the Mueller–Hinton broth medium (Sigma-Aldrich, St. Louis, MO, USA) was placed in each well and 100 μ L of Ag-NPs/BBP (at a concentration of 200 μ g/mg) was placed in the first row of the wells. Serial dilutions were performed to generate the dose–response curve. Control of bacterial growth (only bacteria) and sterility control (broth and NPs) were used. Then, 5 μ L of the respective bacterial suspension was added to each well to perform the inoculation aseptically (the final concentration was approximately 5×10^5 CFU/mL). The tests were performed in triplicate for each strain. The inoculated microplates were incubated at 37 °C for 24 h at 200 RPM. The presence or absence of turbidity in each well was observed. The viable bacteria were determined using a microplate reader (Multiskan GO spectrophotometer, Thermo Scientific, St. Luis, MO, USA) at 595 nm. Samples (5 μ L) of the wells that showed no turbidity were subcultured. **Cytotoxicity assessment.** J774.2 mouse macrophage cells were inoculated (1×10^5 cells/mL) into each well in the 96-well

microplate and incubated for 48 h to achieve complete cell adherence and proliferation. The experiments were performed as described in a previous work carried out by our research team [38]. The Ag-NPs/BBP, diluted in saline solution until they reached a concentration of 100 $\mu\text{g}/\text{mL}$, were put in contact with the cell culture and were incubated for a further 24 h at 37 $^{\circ}\text{C}$, 5% CO_2 , and 95% humidity. After that, 0.2 mg/mL of MTT (Sigma-Aldrich, St. Luis, MO, USA) dissolved in DMEM was added into the wells and the cells were incubated for 6 h. Formazan was dissolved with dimethyl sulfoxide (DMSO, Sigma-Aldrich, St. Louis, MO, USA) [38]. The cell viability determination was performed at 570 nm of optical absorbance with a microplate reader (Multiskan GO spectrophotometer, Thermo Scientific, St. Luis, MO, USA). The cytotoxic classification was determined from the dose–response curve of each sample in triplicate for the three independent experiments, according to ISO 10990-5 [39].

3. Results

3.1. X-ray Diffraction (XRD)

The structural analysis of the system was carried out using the XRD technique. Figure 1 compares the pattern of the pure bovine bone powder (magenta) and the bovine bone powder with Ag-NPs (blue). In the case of the pure bovine bone powder, the pattern shows signals at the 2θ values of 32 $^{\circ}$, 32.3 $^{\circ}$, 46.99 $^{\circ}$, and 49.66 $^{\circ}$ that could be correlated with the planes of hexagonal hydroxyapatite (211), (300), (222), and (213), respectively (ICDD card: 00-086-0740). Likewise, the bovine bone powder with Ag-NPs shows a slight signal at the 2θ value of 38.1 $^{\circ}$ that could be correlated with the plane (111) of FCC Ag (ICDD card: 00-004-0783).

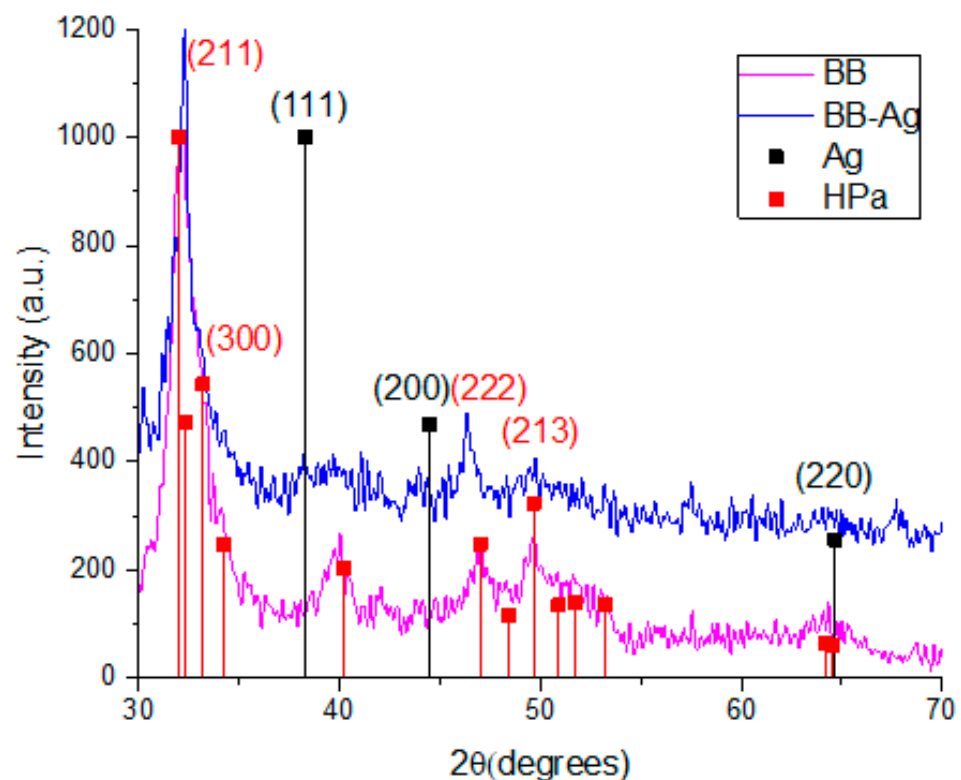


Figure 1. XRD patterns of pure bovine bone powder, BBP (magenta), and Ag-NPs supported on BBP (blue).

3.2. UV–Vis Spectroscopy

In order to characterize the optical response of the nanocomposite of BBP-Ag-NPs, the UV–vis spectroscopy technique was used; it is important to note that, silver nanoparticles can be also detected by other means than this technique. In the inset of Figure 2, the

absorption band of the Ag-NPs supported on BBP (red) is higher than the pure BBP (blue) band, this difference can be attributed to the presence of silver nanoparticles on the sample. It has been reported that the localized surface plasmon resonance (LSPR) of the Ag-NPs is between 400 and 450 nm, depending on the method used for the synthesis, which is generated by the plasmonic resonance of light on the surface of the Ag-NPs [40–42]. In Figure 2, the pure BBP shows no LSPR in this region; however, for the Ag-NPs sample supported on BBP, an absorption peak can be observed at 435 nm; having the nanoparticles supported on BBP and not being an aqueous solution causes the absorbance peak to be less defined. Furthermore, to determinate the band gap of the Ag-NPs, the Tauc model [43,44] was used (Figure 2). The band gap value of the Ag-NPs supported on BBP was 2.19 eV (567 nm) and the pure BBP was 2.42 eV (513 nm), this difference means less energy is required to pass an electron from the valance band to the conduction band in the Ag-NPs nanocomposite. Decreasing the band gap of the nanocomposite leads to an improvement in its photocatalytic [40,45] and photoelectrochemical properties [46].

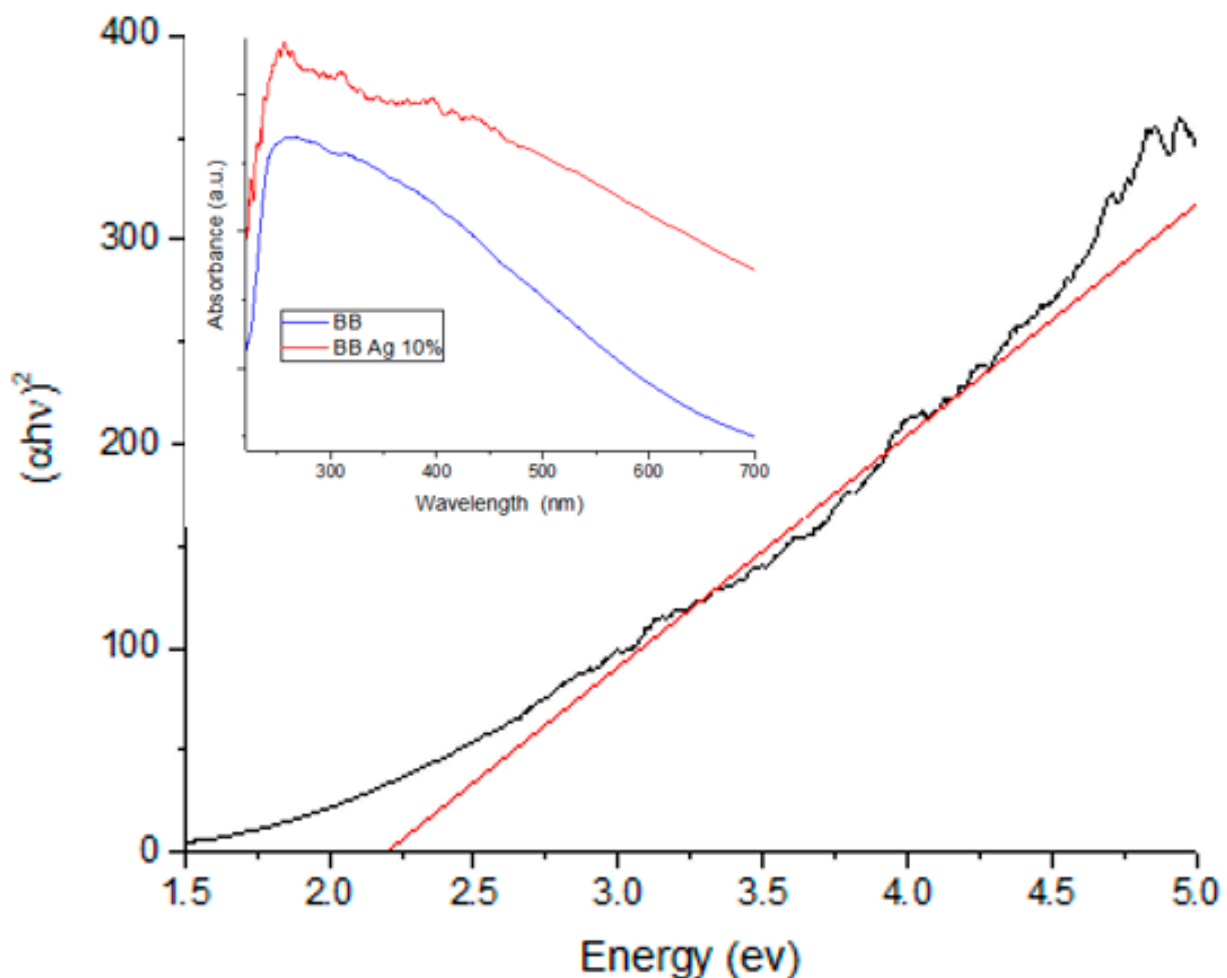


Figure 2. Tauc plot of Ag-NPs supported on BBP sample for band gap value determination; the inset shows the UV-vis spectra of Ag-NPs supported on BBP sample, as well as the bare BBP sample.

3.3. Scanning Electron Microscopy (SEM)

Figure 3 shows the SEM images of the Ag-NPs supported on BBP; it can be noted that an irregular morphology exists due the hydroxyapatite being a porous (220–900 μm) and polycrystalline material; after pulverization treatment, its particles obtained a heterogeneous size and distribution; as is expected, in the SEM image it was not possible to observe the silver nanoparticles.

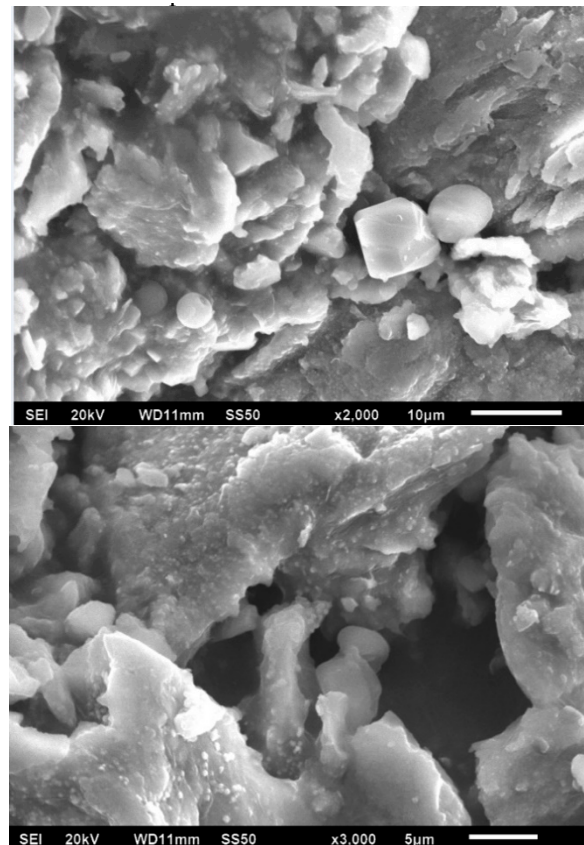


Figure 3. SEM images of Ag-NPs supported on BBP, 20 kV.

Furthermore, Figure 4 shows the results of the EDS elemental analysis of the composition of the nanocomposite; in the first place, the support is mainly composed of hydroxyapatite ($\text{Ca}_5(\text{PO}_4)_3(\text{OH})_2$), and elements such as oxygen, carbon, phosphorus, and calcium were detected; it has been reported that bovine bone powder contains small amounts of Mg^+ [47,48]; also, silver was identified. Moreover, elemental mapping (Figure 5) shows the distribution of the elements in the nanocomposite; silver, specifically, has a homogeneous distribution over the support.

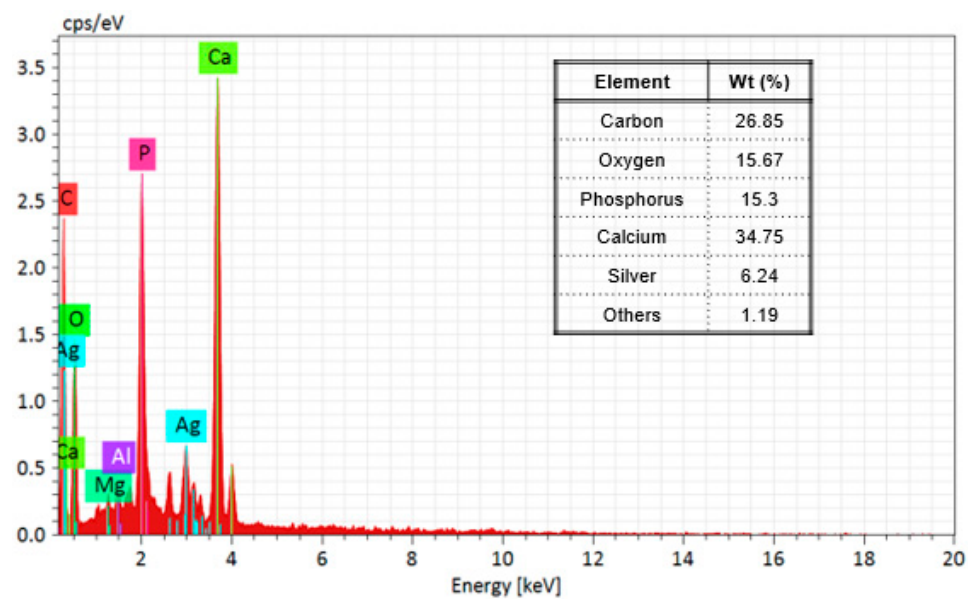


Figure 4. EDS spectrum and table of mass % elemental composition of Ag-NPs supported on BBP.

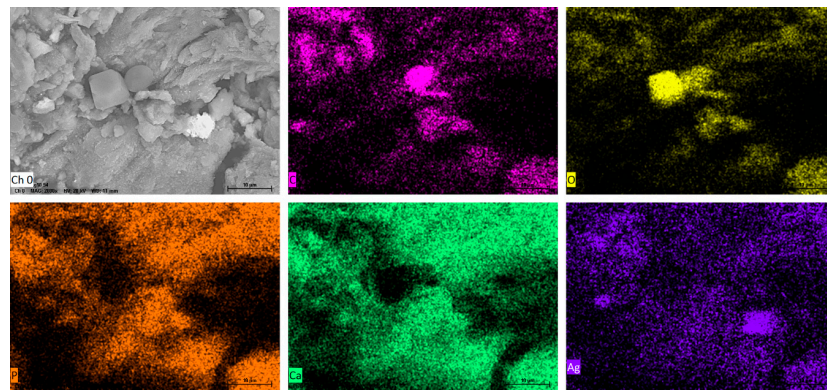


Figure 5. EDS elemental mapping of SEM of Ag-NPs supported on BBP; Ch (O) surface of Ag-NPs supported on BBP before mapping; mapping of (C) carbon, (O) oxygen, (P) phosphorus (Ca) calcium, and (Ag) silver.

3.4. Transmission Electron Microscopy (TEM)

Figure 6a,b shows the transmission electron microscopy images of the Ag-NPs supported on BBP; as can be seen, the round darker zones can be attributed to silver particles, whereas the brighter zones can be related to the bovine bone support; the silver particles show good polydispersity, with a size range between 5 and 57 nm and a quasi-spherical shape. It is worth mentioning that Ag-NPs seem to be supported on the bovine bone matrix even after being sonicated for a period of 5 h. The average size of the Ag-NPs was 22.6 nm, according to the measurement of approximately 675 particles (Figure 7). Figure 6d shows the selected-area electron diffraction (SAED) of Ag-NPs supported on BBP; the interplanar distance between the atoms was measured; the SAED patterns were indexed corresponding to the (111) Ag lattice planes, according to the FCC structure (ICDD pattern: 00-004-0783) and (002), (211), (222), and (213) hydroxyapatite lattice planes, according to a hexagonal structure (ICDD pattern: 00-086-0740). The results obtained through the TEM technique confirm that the Ag-NPs synthesized using *Heterotheca inuloides* were obtained, have a good polydispersity, an average size of 22.6 nm, and have a good link with the bovine bone due to the electrostatic forces.

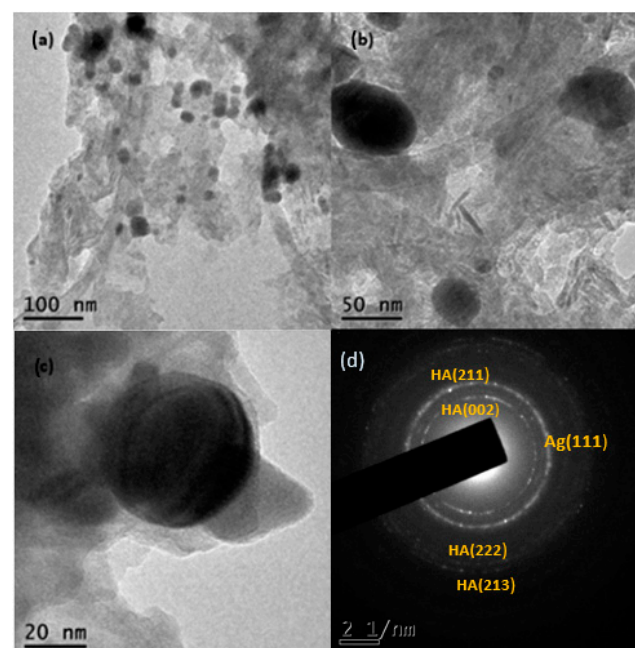


Figure 6. (a,b) TEM micrographs of Ag-NPs supported on BBP, (c) Ag nanoparticle on BBP, and (d) SAED pattern, respectively.

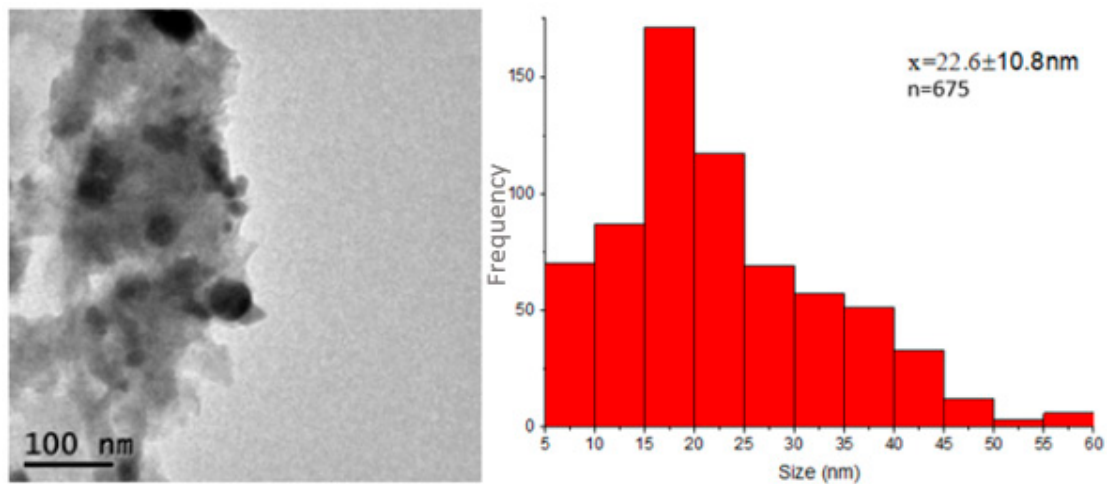


Figure 7. Size distribution histogram of Ag-NPs supported on BBP, constructed from TEM observations.

3.5. Fourier Transform Infrared Spectroscopy (FTIR)

The blue spectrum in Figure 8 corresponds to the Ag-NPs supported on BBP (red) and the bare BBP (blue); the spectrum shows peaks with different intensities, representing different chemical bonds of the molecules that compose the samples. The most significant peaks of the bovine bone powder are found at 2970 cm^{-1} (CH_2 asymmetric stretch), 1445 cm^{-1} , and 1414 cm^{-1} (CH_2 wagging and bending vibrations and CO_3^{2-}), 1016 cm^{-1} (PO_4^{3-} asymmetric stretch), 873 cm^{-1} (CO_3^{2-} bending vibrations), 600 cm^{-1} , and 560 cm^{-1} (PO_4^{3-} bending vibrations), these functional groups are characteristic of hydroxyapatite and collagen, the main components of bovine bone powder [49,50]. Likewise, in Figure 8, the Ag nanoparticles supported on BBP sample (red spectrum), minor peaks were found at the following wavelengths, 1375 cm^{-1} (C-O stretch), 1535 cm^{-1} (C=C-C stretch), and 2924 cm^{-1} (CH stretch, OH^- stretch of aliphatic acids), which can be attributed to the functional groups corresponding to polyphenols, phenols, and sesquiterpene compounds [51–53]. Moreover, comparing the Ag-BBP (red) and bare BBP (blue) spectra, it is possible to observe a decrease in the peaks at 600 cm^{-1} , 560 cm^{-1} and 1016 cm^{-1} , corresponding to PO_4^{3-} functional groups of hydroxyapatite, and 1445 cm^{-1} and 1414 cm^{-1} corresponding to CO_3^{2-} groups of collagen. This modification can be associated with the interaction between Ag nanoparticles and the bovine bone powder, the changes mainly occurred in the PO_4^{3-} groups; this interaction does not allow the bonded molecules to vibrate as easily, producing a decrease in their peak.

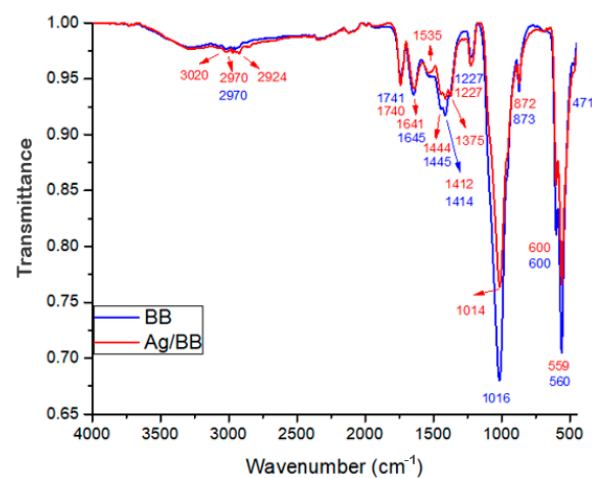


Figure 8. FTIR spectrum of Ag-NPs supported on BBP sample (red), as well as the bare BBP sample (blue).

3.6. Antibacterial Evaluation

Table 1 and Figure 9 show the results of the antibacterial test. The minimal inhibitory concentrations (MICs) of the Ag-NPs/BBP against the tested strains were determined by the wells that showed no turbidity. The MICs for *S. aureus*, *E. coli*, and *S. epidermidis* were 6.25, 12.5, and 6.25%, respectively. The MBCs of the Ag-NPs/BBP for *S. aureus*, *E. coli*, and *S. epidermidis* were 12.5, 50, and 25% respectively. The bare bovine bone powder has no antibacterial effect.

Table 1. Results of microdilution broth test on Ag-NPs/BBP at different dilutions against the tested strains.

Serial Dilution (µg/mL)	<i>S. aureus</i>	<i>E. coli</i>	<i>S. epidermidis</i>
0	100.00 ± 2.2	100.00 ± 5.3	100.00 ± 4.9
0.390625	82.77 ± 5.1	83.58 ± 4.6	74.19 ± 2.5
0.78125	70.39 ± 3.2	84.08 ± 3.6	54.42 ± 4.6
1.5625	62.62 ± 4.3	85.07 ± 5.0	55.35 ± 5.1
3.125	63.35 ± 2.9	71.64 ± 4.2	55.12 ± 4.3
6.25	12.38 ± 3.1	23.88 ± 3.1	5.58 ± 1.7
12.5	0.01 ± 0.1	10.45 ± 1.8	6.51 ± 1.2
25	0.00 ± 0.0	5.42 ± 0.9	0.01 ± 0.0
50	0.00 ± 0.0	0.00 ± 0.0	0.00 ± 0.0

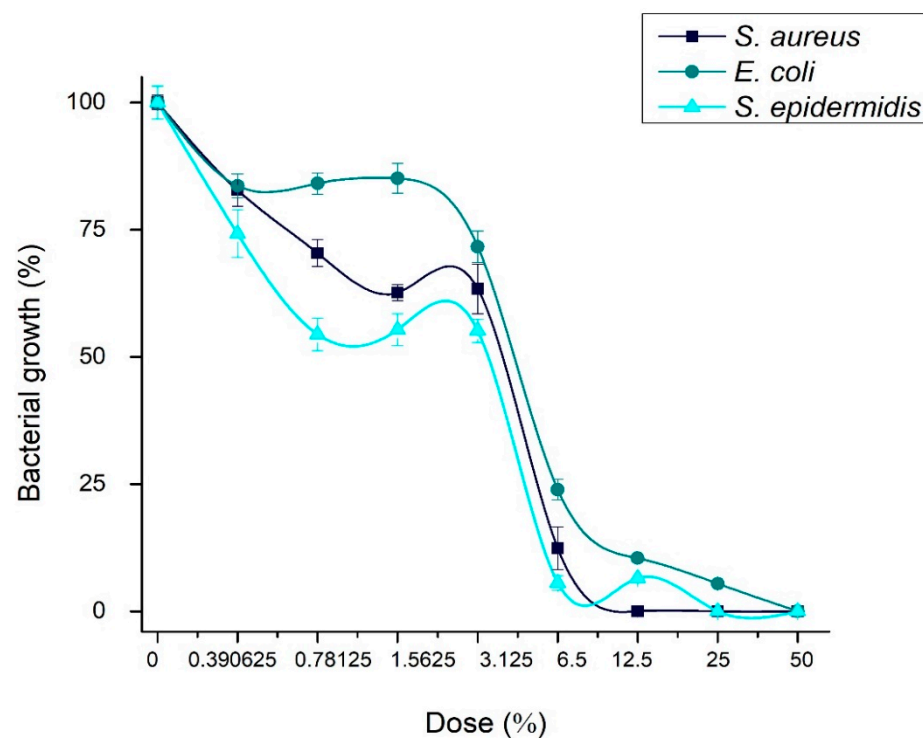


Figure 9. Concentration of bacterial growth in presence of Ag-NPs/BBP at different dilutions against the strains studied.

S. epidermidis and *S. aureus* are gram-positive bacteria; although, the latter in a clinical context has been shown to have drug resistance; on the other hand, *S. epidermidis* proliferates and causes infections in hospitalized or immunosuppressed patients; in addition to having a great capacity to form biofilms, which is its main mechanism of resistance. Apparently, being gram positive, both strains showed similar susceptibility (MICs) to the different concentrations of the Ag-NPs/BBP tested.

3.7. Cytotoxic Evaluation

The results of the J774.2 mouse macrophage cell viability in direct contact with Ag-NPs/BBP are shown in Table 2 and Figure 10. It had been hypothesized that the hydroxyl groups (OH^-) of the polyphenols and other biomolecules from the *Heterotheca inuloides* infusion could lead to the stabilization and reduction of silver ions (Ag^+) to Ag_0 , and that some of these biomolecules may stay on the surface of the nanoparticles, contributing to the enhanced biocompatibility of the same [54]. In chemical reduction synthesis, it is possible that part of the silver nitrate ions that remain unreacted, as well as residues of the reducing agent, such as sodium borohydride, contribute to greater cytotoxicity [55]. In addition, another factor that has been associated with cytotoxicity is particle size, since nanoparticles smaller than 20 nm are more likely to be internalized in the cell. In the current work, cytotoxicity was rated in accordance with ISO standard 10993-5 [41] as non-cytotoxic (cell viability higher than 75%), slightly cytotoxic (cell viability ranging from 50% to 75%), moderately cytotoxic (cell viability ranging from 25% to 50%), and severely cytotoxic (cell viability lower than 25%) [38]. Then, 50 and 25% dilutions of Ag-NPs/BBP resulted in being moderately cytotoxic, 12.5 and 6.25% were slightly cytotoxic, whereas 3.125, 1.5625, and 0.78125% were non-cytotoxic.

Table 2. Cytotoxic evaluation results for Ag-NPs/BBP, at different dilutions, performed on J774.2 mouse macrophage cells.

Serial Dilution ($\mu\text{g/mL}$)	Relative Cell Viability (%Mean \pm SD)
0	100.00 \pm 2.0
0.78125	94.78 \pm 1.7
1.5625	83.26 \pm 2.5
3.125	78.37 \pm 1.7
6.25	64.07 \pm 4.2
12.5	53.70 \pm 2.9
25	40.10 \pm 0.7
50	29.10 \pm 0.8

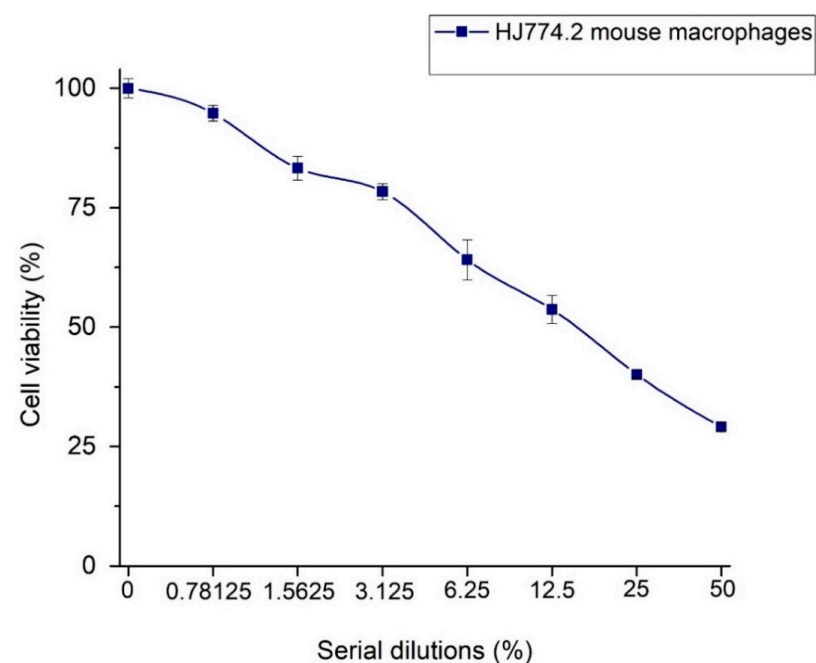


Figure 10. Relative cell viability of J774.2 mouse macrophage cells in direct contact with Ag-NPs/BBP.

4. Discussion

The results of the characterization confirm the presence of Ag nanoparticles supported on bovine bone powder; the SEM and TEM techniques prove the presence of hydroxyapatite and collagen, and elements like C, O, P, and Ca were detected, likewise, small amounts of Mg were detected; the presence of silver was analyzed by EDS, XRD, and TEM; TEM microscopy showed the size of the silver nanoparticles (22.6 ± 10.8 nm) and good polydispersity over the BBP. Crystalline analysis of the Ag-NPs showed correspondence to (111) Ag lattice planes, according to the FCC structure (XRD and TEM). The Ag-NPs supported on BBP showed a decrease in the band gap (2.19 eV) compared with pure BBP (2.42 eV) (UV-Vis), which could improve the catalytic activity in the near to visible range of the electromagnetic spectrum FTIR, showing that the Ag-NPs are bound to the PO_4^{3-} and CO_3^{2-} functional groups of the BBP by considerably decreasing the intensity of their peak, as the binding of the functional groups to the Ag-NPs does not allow the molecule to vibrate freely, which decreases the energy transmittance. On the other hand, it was possible to detect small transmittance peaks corresponding to the functional groups present in phenols, polyphenols, and sesquiterpene compounds, these compounds are present in the composition of *Heterotheca inuloides*, which indicates that the Ag/BBP composite is impregnated with small amounts of organic compounds present in *Heterotheca inuloides*.

According to the above results, it can be proved that phenols, polyphenols, and sesquiterpene compounds from the leaves and flowers of *Heterotheca inuloides* are able to reduce Ag^{+1} to Ag^0 , forming nanometer-sized nanoparticles on the surface of bovine bone powder; the PO_4^{3-} and CO_3^{2-} functional groups of BBP form a bond with Ag-NPs.

The effect of pH on silver nanoparticles has been studied, showing that in a short-term study at a lower pH of the solution (4), the size of the nanoparticles increases; on the other hand, as the pH of the solution increases, the size of the nanoparticles decreases; on the other hand, in a long-term study, the size of the nanoparticles increased at different pH; this study was carried out in an aqueous solution [56,57]; in the case of the Ag-NPs/BBP system, further studies will be carried out to determine how pH affects the properties of Ag-NPs when supported on BBP.

Although Ag-NPs have been extensively studied, they remain one of the most controversial areas of research regarding their mechanism of action over different strains. Current evidence indicates that the release of extracellular and intracellular ions is a mechanism that acts simultaneously with the intracellular deposition of the nanoparticles [58]. Likewise, the release of reactive oxygen species intra and extracellular by the silver nanoparticles generates oxidative stress inside the bacterial cell [59].

The inhibitory action mechanism has been described according to the electronegative attraction of the sulfate and phosphate (−) groups in the bacteria cell membrane to the Ag (+) ions that could be released from Ag-NPs. This interaction could interfere with the permeability and respiration of the bacteria, obstructing its capacity of replicate, ending in the protein denaturation of the bacteria [54,60–63].

The *S. epidermidis* and *S. aureus* (gram-positive bacteria), and *E. coli* (gram-negative bacteria), MIC was determined; gram-positive bacteria showed similar susceptibility to the Ag-NPs, the concentration being lower than gram-negative bacteria, this is due to the type of cell membranes of which they are composed.

Studies on cell lines, such as HepG2, and macrophages have shown that toxicity depends on the size of the nanoparticle and is due to the production of oxidative stress that leads to cell death due to apoptosis. J774 cells are more sensitive due to their intrinsic capacity in the ROS production mechanism compared to other cell lines. The MTT results were used as an indication of ROS production because the mechanism of action of silver nanoparticles is through the disruption of the cell membrane, the internment of the nanoparticles into the cytoplasm, and their interaction with the cell nucleus causing DNA destruction. In addition, the formation of free radicals, both ROS and RNS, causing oxidative stress and damage to cellular macromolecules (carbohydrates, lipids, proteins, and nucleic acids) also occurs [64].

The minimum Inhibitory concentration (MIC) of Ag-NPs for *E. coli*, *S. epidermidis*, and *S. aureus* bacteria shows a slight cytotoxicity.

5. Conclusions

The synthesis of silver nanoparticles using natural reducers and supports is a viable solution to actual environmental and health problems. Bovine bone powder is an ecofriendly, cheap, and renewable material. It is an inert material, acts as an excipient, with a high electronic density provided by PO_4^{3-} and CO_3^{2-} functional groups; these groups are the ones that anchor the metal ions to the support (FTIR). An infusion of *Heterotheca inuloides* leaves and flowers can reduce Ag^{+1} to Ag^0 , due to the reductive potential of polyphenol, phenol, and sesquiterpene compounds presents in the plant. Through characterization, the obtaining of the nanocomposite was proved, an elemental composition study was carried out by SEM, and elements like C, O, P, Ca (hydroxyapatite ($\text{Ca}_5(\text{PO}_4)_3(\text{OH})_2$)), and Ag were detected; the UV–Vis spectroscopy characterization showed the presence of the silver plasmon and a decrease in the band gap from 2.42 eV (pure BBP) to 2.19 eV (Ag-NPs/BBP); the decrease in the band gap of the Ag-NPs/BBP composite means that there is an improvement in its photocatalytic properties. The TEM observations confirmed the formation of Ag-NPs with an almost unimodal and slightly wide particle size distribution, with an average size of $22.6 \text{ nm} \pm 10.8 \text{ nm}$ and a quasi-spherical shape. The XRD analysis showed the presence (111) Ag lattice planes, according to the FCC structure, and an average crystal size of 20.62 nm. The MICs for *S. aureus*, *E. coli*, and *S. epidermidis* were 6.25, 12.5, and 6.25%, respectively. Moreover, the concentrations $\leq 12.5\%$ were slightly cytotoxic or non-cytotoxic. Based on the results, this system has potential applications in the medicine and food industries. This research found that the facile and ecofriendly synthesis of Ag-NPs supported on bovine bone powder resulted in an effective bactericidal system against the strains studied, without significant cytotoxicity.

Author Contributions: Conceptualization, A.R.V.-N., A.M.-R., L.A.-F. and S.A.G.-L.; methodology, S.A.G.-L., A.R.V.-N., A.M.-R., M.S.P.-M., M.A.Z.-A. and L.A.-F.; validation, S.A.G.-L. formal analysis, S.A.G.-L., A.R.V.-N., A.M.-R. and L.A.-F.; investigation, S.A.G.-L.; resources, S.A.G.-L.; data curation, S.A.G.-L., A.M.-R., L.A.-F., M.A.Z.-A. and A.R.V.-N.; writing—original draft preparation, S.A.G.-L., A.M.-R., L.A.-F. and A.R.V.-N.; writing—review and editing, S.A.G.-L. All authors have read and agreed to the published version of the manuscript.

Funding: This research received no external funding.

Data Availability Statement: The data presented in this study are available on request from the corresponding author. The raw data required to reproduce these findings cannot be shared at this time as the data also forms part of an ongoing study.

Acknowledgments: The authors would like to thank Alejandro Parada Flores and Isaura Itzel Acosta Sánchez for their technical contributions.

Conflicts of Interest: The authors declare no conflicts of interest.

References

1. Bouafia, A.; Laouini, S.E.; Ahmed, A.S.; Soldatov, A.V.; Algarni, H.; Feng Chong, K.; Ali, G.A. The recent progress on silver nanoparticles: Synthesis and electronic applications. *Nanomaterials* **2021**, *11*, 2318. [\[CrossRef\]](#)
2. Espinosa-Cristóbal, L.F.; Martínez-Castañón, G.A.; Martínez-Martínez, R.E.; Loyola-Rodriguez, J.P.; Patino-Marin, N.; Reyes-Macias, J.F.; Ruiz, F. Antibacterial effect of silver nanoparticles against *Streptococcus mutans*. *Mater. Lett.* **2009**, *63*, 2603–2606. [\[CrossRef\]](#)
3. Salayová, A.; Bedlovičová, Z.; Daneu, N.; Baláž, M.; Lukáčová Bujňáková, Z.; Balážová, L.; Tkáčiková, L. Green synthesis of silver nanoparticles with antibacterial activity using various medicinal plant extracts: Morphology and antibacterial efficacy. *Nanomaterials* **2021**, *11*, 1005. [\[CrossRef\]](#)
4. Wen, L.; Zeng, P.; Zhang, L.; Huang, W.; Wang, H.; Chen, G. Symbiosis theory-directed green synthesis of silver nanoparticles and their application in infected wound healing. *Int. J. Nanomed.* **2016**, *11*, 2757.
5. Naz, M.; Nasiri, N.; Ikram, M.; Nafees, M.; Qureshi, M.Z.; Ali, S.; Tricoli, A. Eco-friendly biosynthesis, anticancer drug loading and cytotoxic effect of capped Ag-nanoparticles against breast cancer. *Appl. Nanosci.* **2017**, *7*, 793–802. [\[CrossRef\]](#)

6. de Jesús Ruíz-Baltazar, Á.; Reyes-López, S.Y.; de Lourdes Mondragón-Sánchez, M.; Estevez, M.; Hernández-Martínez, A.R.; Pérez, R. Biosynthesis of Ag nanoparticles using *Cynara cardunculus* leaf extract: Evaluation of their antibacterial and electrochemical activity. *Results Phys.* **2018**, *11*, 1142–1149. [[CrossRef](#)]
7. Nakkala, J.R.; Mata, R.; Gupta, A.K.; Sadras, S.R. Biological activities of green silver nanoparticles synthesized with *Acorus calamus* rhizome extract. *Eur. J. Med. Chem.* **2014**, *85*, 784–794. [[CrossRef](#)]
8. Ibrahim, H.M. Green synthesis and characterization of silver nanoparticles using banana peel extract and their antimicrobial activity against representative microorganisms. *J. Radiat. Res. Appl. Sci.* **2015**, *8*, 265–275. [[CrossRef](#)]
9. Zhao, Y.; Yang, X.; Tian, J.; Wang, F.; Zhan, L. Methanol electro-oxidation on Ni@ Pd core-shell nanoparticles supported on multi-walled carbon nanotubes in alkaline media. *Int. J. Hydrogen Energy* **2010**, *35*, 3249–3257. [[CrossRef](#)]
10. Siamaki, A.R.; Abd El Rahman, S.K.; Abdelsayed, V.; El-Shall, M.S.; Gupton, B.F. Microwave-assisted synthesis of palladium nanoparticles supported on graphene: A highly active and recyclable catalyst for carbon–carbon cross-coupling reactions. *J. Catal.* **2011**, *279*, 1–11. [[CrossRef](#)]
11. Wu, G.H.; Wu, Y.F.; Liu, X.W.; Rong, M.C.; Chen, X.M.; Chen, X. An electrochemical ascorbic acid sensor based on palladium nanoparticles supported on graphene oxide. *Anal. Chim. Acta* **2012**, *745*, 33–37. [[CrossRef](#)] [[PubMed](#)]
12. Shekhar, M.; Wang, J.; Lee, W.S.; Williams, W.D.; Kim, S.M.; Stach, E.A.; Miller, J.T.; Delgass, W.N.; Ribeiro, F.H. Size and support effects for the water–gas shift catalysis over gold nanoparticles supported on model Al₂O₃ and TiO₂. *J. Am. Chem. Soc.* **2012**, *134*, 4700–4708. [[CrossRef](#)] [[PubMed](#)]
13. Lee, B.; Ma, Z.; Zhang, Z.; Park, C.; Dai, S. Influences of synthesis conditions and mesoporous structures on the gold nanoparticles supported on mesoporous silica hosts. *Microporous Mesoporous Mater.* **2009**, *122*, 160–167. [[CrossRef](#)]
14. Moon, R.J.; Martini, A.; Nairn, J.; Simonsen, J.; Youngblood, J. Cellulose nanomaterials review: Structure, properties and nanocomposites. *Chem. Soc. Rev.* **2011**, *40*, 3941–3994. [[CrossRef](#)] [[PubMed](#)]
15. Nan, H.; Tian, X.; Yang, L.; Shu, T.; Song, H.; Liao, S. A platinum monolayer core-shell catalyst with a ternary alloy nanoparticle core and enhanced stability for the oxygen reduction reaction. *J. Nanomater.* **2015**, *2015*, 715474. [[CrossRef](#)]
16. Morales-Luckie, R.A.; Lopezfuentes-Ruiz, A.A.; Olea-Mejía, O.F.; Liliana, A.F.; Sanchez-Mendieta, V.; Brostow, W.; Hinestroza, J.P. Synthesis of silver nanoparticles using aqueous extracts of *Heterotheca inuloides* as reducing agent and natural fibers as templates: *Agave lechuguilla* and silk. *Mater. Sci. Eng. C* **2016**, *69*, 429–436. [[CrossRef](#)] [[PubMed](#)]
17. Haji, A.; Barani, H.; Qavamnia, S.S. In situ synthesis of silver nanoparticles onto cotton fibres modified with plasma treatment and acrylic acid grafting. *Micro Nano Lett.* **2013**, *8*, 315–318. [[CrossRef](#)]
18. Rodrigues, C.V.M.; Serricella, P.; Linhares, A.B.R.; Guerdes, R.M.; Borojevic, R.; Rossi, M.A.; Duarte, M.E.L.; Farina, M. Characterization of a bovine collagen–hydroxyapatite composite scaffold for bone tissue engineering. *Biomaterials* **2003**, *24*, 4987–4997. [[CrossRef](#)]
19. Hing, K.A.; Best, S.M.; Bonfield, W. Characterization of porous hydroxyapatite. *J. Mater. Sci. Mater. Med.* **1999**, *10*, 135–145. [[CrossRef](#)]
20. Bee, S.L.; Bustami, Y.; Ul-Hamid, A.; Lim, K.; Abdul Hamid, Z.A. Synthesis of silver nanoparticle-decorated hydroxyapatite nanocomposite with combined bioactivity and antibacterial properties. *J. Mater. Sci. Mater. Med.* **2021**, *32*, 106. [[CrossRef](#)]
21. Bee, S.L.; Bustami, Y.; Ul-Hamid, A.; Hamid, Z.A. Green biosynthesis of hydroxyapatite-silver nanoparticle nanocomposite using aqueous Indian curry leaf (*Murraya koenigii*) extract and its biological properties. *Mater. Chem. Phys.* **2022**, *277*, 125455. [[CrossRef](#)]
22. Almajano, M.P.; Carbo, R.; Jiménez, J.A.L.; Gordon, M.H. Antioxidant and antimicrobial activities of tea infusions. *Food Chem.* **2008**, *108*, 55–63. [[CrossRef](#)]
23. Raja, P.B.; Rahim, A.A.; Qureshi, A.K.; Awang, K. Green synthesis of silver nanoparticles using tannins. *Mater. Sci.-Pol.* **2014**, *32*, 408–413. [[CrossRef](#)]
24. Singhal, G.; Bhavesh, R.; Kasariya, K.; Sharma, A.R.; Singh, R.P. Biosynthesis of silver nanoparticles using *Ocimum sanctum* (Tulsi) leaf extract and screening its antimicrobial activity. *J. Nanoparticle Res.* **2011**, *13*, 2981–2988. [[CrossRef](#)]
25. Haghghi Pak, Z.; Abbaspour, H.; Karimi, N.; Fattahi, A. Eco-friendly synthesis and antimicrobial activity of silver nanoparticles using *Dracocephalum moldavica* seed extract. *Appl. Sci.* **2016**, *6*, 69. [[CrossRef](#)]
26. Kaviya, S.; Santhanalakshmi, J.; Viswanathan, B.; Muthumary, J.; Srinivasan, K. Biosynthesis of silver nanoparticles using *Citrus sinensis* peel extract and its antibacterial activity. *Spectrochim. Acta Part A Mol. Biomol. Spectrosc.* **2011**, *79*, 594–598. [[CrossRef](#)] [[PubMed](#)]
27. Baharara, J.; Namvar, F.; Ramezani, T.; Hosseini, N.; Mohamad, R. Green synthesis of silver nanoparticles using *Achillea biebersteinii* flower extract and its anti-angiogenic properties in the rat aortic ring model. *Molecules* **2014**, *19*, 4624–4634. [[CrossRef](#)] [[PubMed](#)]
28. Shaik, M.; Khan, M.; Kuniyil, M.; Al-Warthan, A.; Alkhatlan, H.; Siddiqui, M.; Shaik, J.P.; Ahamed, A.; Mahmood, A.; Khan, M.; et al. Plant-extract-assisted green synthesis of silver nanoparticles using *Origanum vulgare* L. extract and their microbicidal activities. *Sustainability* **2018**, *10*, 913. [[CrossRef](#)]
29. Rodríguez-Chávez, J.L.; Egas, V.; Linares, E.; Bye, R.; Hernández, T.; Espinosa-García, F.J.; Delgado, G. Mexican Arnica (*Heterotheca inuloides* Cass. Asteraceae: Astereae): Ethnomedical uses, chemical constituents and biological properties. *J. Ethnopharmacol.* **2017**, *195*, 39–63. [[CrossRef](#)]
30. Delgado, G.; del Socorro Olivares, M.; Chávez, M.I.; Ramírez-Apan, T.; Linares, E.; Bye, R.; Espinosa-García, F.J. Antiinflammatory Constituents from *Heterotheca inuloides*. *J. Nat. Prod.* **2001**, *64*, 861–864. [[CrossRef](#)]

31. del Puerto Horta, M.; Casas Insua, L.; Cañete Villafranca, R. Usos más frecuentes de *Arnica montana*. *Rev. Cuba. Plantas Med.* **2013**, *18*, 315–326.
32. Gené, R.M.; Segura, L.; Adzet, T.; Marin, E.; Iglesias, J. *Heterotheca inuloides*: Anti-inflammatory and analgesic effect. *J. Ethnopharmacol.* **1998**, *60*, 157–162. [[CrossRef](#)] [[PubMed](#)]
33. Hernández-Gómora, A.E.; Lara-Carrillo, E.; Robles-Navarro, J.B.; Scougall-Vilchis, R.J.; Hernández-López, S.; Medina-Solís, C.E.; Morales-Luckie, R.A. Biosynthesis of silver nanoparticles on orthodontic elastomeric modules: Evaluation of mechanical and antibacterial properties. *Molecules* **2017**, *22*, 1407. [[CrossRef](#)] [[PubMed](#)]
34. Gama-Lara, S.A.; Natividad, R.; Vilchis-Nestor, A.R.; López-Castañares, R.; García-Orozco, I.; Gonzalez-Pedroza, M.G.; Morales-Luckie, R.A. Ultra-small platinum nanoparticles with high catalytic selectivity synthesized by an eco-friendly method supported on natural hydroxyapatite. *Catal. Lett.* **2019**, *149*, 3447–3453. [[CrossRef](#)]
35. Mijangos Ricárdez, O.F.; Ruiz-Jiménez, J.; Lagunez-Rivera, L.; Luque de Castro, M.D. Fast Ultrasound-assisted Extraction of Polar (phenols) and Nonpolar (lipids) Fractions in *Heterotheca inuloides* Cass. *Phytochem. Anal.* **2011**, *22*, 484–491. [[CrossRef](#)] [[PubMed](#)]
36. Gama-Lara, S.A.; Morales-Luckie, R.; Argueta-Figueroa, L.; Hinestroza, J.P.; García-Orozco, I.; Natividad, R. Synthesis, characterization, and catalytic activity of platinum nanoparticles on bovine-bone powder: A novel support. *J. Nanomater.* **2018**, *2018*, 6482186. [[CrossRef](#)]
37. Torres-Gómez, N.; Nava, O.; Argueta-Figueroa, L.; García-Contreras, R.; Baeza-Barrera, A.; Vilchis-Nestor, A.R. Shape Tuning of Magnetite Nanoparticles Obtained by Hydrothermal Synthesis: Effect of Temperature. *J. Nanomater.* **2019**, *2019*, 7921273. [[CrossRef](#)]
38. Argueta-Figueroa, L.; Torres-Gómez, N.; García-Contreras, R.; Vilchis-Nestor, A.; Martínez-Alvarez, O.; Acosta-Torres, L.; Arenas-Arrocena, M. Hydrothermal synthesis of pyrrhotite (Fex-1S) nanoplates and their antibacterial, cytotoxic activity study. *Prog. Nat. Sci. Mater. Int.* **2018**, *28*, 447–455. [[CrossRef](#)]
39. ISO 10993-5:2009; Biological Evaluation of Medical Devices-Part 5: Tests for In Vitro Cytotoxicity. International Organization for Standardization: Geneva, Switzerland, 2009; pp. 1–34.
40. Sarina, S.; Waclawik, E.R.; Zhu, H. Photocatalysis on supported gold and silver nanoparticles under ultraviolet and visible light irradiation. *Green Chem.* **2013**, *15*, 1814–1833. [[CrossRef](#)]
41. Oros-Ruiz, S.; Zanella, R.; Prado, B. Photocatalytic degradation of trimethoprim by metallic nanoparticles supported on TiO₂-P25. *J. Hazard. Mater.* **2013**, *263*, 28–35. [[CrossRef](#)]
42. Kelly, K.L.; Coronado, E.; Zhao, L.L.; Schatz, G.C. The optical properties of metal nanoparticles: The influence of size, shape, and dielectric environment. *J. Phys. Chem. B* **2003**, *107*, 668–677. [[CrossRef](#)]
43. Luque, P.A.; Garrafa-Gálvez, H.E.; Nava, O.; Olivas, A.; Martínez-Rosas, M.E.; Vilchis-Nestor, A.R.; Villegas-Fuentes, A.; Chinchillas-Chinchillas, M.J. Efficient sunlight and UV photocatalytic degradation of Methyl Orange, Methylene Blue and Rhodamine B, using Citrus × paradisi synthesized SnO₂ semiconductor nanoparticles. *Ceram. Int.* **2021**, *47*, 23861–23874. [[CrossRef](#)]
44. Muhammed, D.S.; Brza, M.A.; M. Nofal, M.; B. Aziz, S.; A. Hussien, S.; Abdulwahid, R.T. Optical dielectric loss as a novel approach to specify the types of electron transition: XRD and UV-vis as a non-destructive techniques for structural and optical characterization of PEO based nanocomposites. *Materials* **2020**, *13*, 2979. [[CrossRef](#)] [[PubMed](#)]
45. Tsvetkov, M.; Zaharieva, J.; Milanova, M. Ferrites, modified with silver nanoparticles, for photocatalytic degradation of malachite green in aqueous solutions. *Catal. Today* **2020**, *357*, 453–459. [[CrossRef](#)]
46. Sukomboon, M.; Kongsawatvoragul, K.; Duangdangchote, S.; Sawangphruk, M. Reducing the energy band gap of cobalt hydroxide nanosheets with silver atoms and enhancing their electrical conductivity with silver nanoparticles. *ACS Omega* **2021**, *6*, 20804–20811. [[CrossRef](#)] [[PubMed](#)]
47. Von Euw, S.; Wang, Y.; Laurent, G.; Drouet, C.; Babonneau, F.; Nassif, N.; Azais, T. Bone mineral: New insights into its chemical composition. *Sci. Rep.* **2019**, *9*, 8456. [[CrossRef](#)] [[PubMed](#)]
48. Ojo, O.; Sekunowo, I.; Ilomuanya, M.; Gbenedor, P.; Adeosun, S. Compositions and thermo-chemical analysis of bovine and caprine bones. *Kufa J. Eng.* **2021**, *12*, 56–68. [[CrossRef](#)]
49. Figueiredo, M.M.; Gamelas, J.A.F.; Martins, A.G. Characterization of bone and bone-based graft materials using FTIR spectroscopy. In *Infrared Spectroscopy-Life and Biomedical Sciences*; BoD—Books on Demand: Norderstedt, Germany, 2012; pp. 315–338.
50. Ramesh, S.T.; Rameshbabu, N.; Gandhimathi, R.; Nidheesh, P.V.; Srikanth Kumar, M. Kinetics and equilibrium studies for the removal of heavy metals in both single and binary systems using hydroxyapatite. *Appl. Water Sci.* **2012**, *2*, 187–197. [[CrossRef](#)]
51. Guadarrama-Reyes, S.C.; Morales-Luckie, R.A.; Sánchez-Mendieta, V.; González-Pedroza, M.G.; Lara-Carrillo, E.; Velazquez-Enriquez, U.; Toral-Rizo, V.; Scougall-Vilchis, R. Green synthesis of silver nanoparticles using *Heterotheca inuloides* and its antimicrobial activity in catgut suture threads. In *Engineered Nanomaterials-Health and Safety*; IntechOpen: London, UK, 2019.
52. Dobrucka, R. The biological synthesis of anatase titanium dioxide nanoparticles using *Arnicae anthodium* extract. *Bulg. Chem. Commun* **2017**, *49*, 595–599.
53. Morales-Luckie, R.A.; Palacios-Lozano, S.L.; Sánchez-Mendieta, V.; Olea-Mejia, O.F.; González-Pedroza, M.G. Bionanocomposite of Ag Nanoparticles/Jute Fibers as an Efficient Fungi-Free Material for the Automobile Industry. In *Vegetable Fiber Composites and Their Technological Applications*; Springer: Singapore, 2021; pp. 327–338.
54. Alharbi, N.S.; Alsubhi, N.S.; Felimban, A.I. Green synthesis of silver nanoparticles using medicinal plants: Characterization and application. *J. Radiat. Res. Appl. Sci.* **2022**, *15*, 109–124. [[CrossRef](#)]

55. Wolny-Kołodka, K.; Malina, D.; Suder, A.; Pluta, K.; Wzorek, Z. Bio-based synthesis of silver nanoparticles from waste agricultural biomass and its antimicrobial activity. *Processes* **2022**, *10*, 389. [[CrossRef](#)]
56. Fernando, I.; Zhou, Y. Impact of pH on the stability, dissolution and aggregation kinetics of silver nanoparticles. *Chemosphere* **2019**, *216*, 297–305. [[CrossRef](#)]
57. Fernando, K.M.; Gunathilake, C.A.; Yalegama, C.; Samarakoon, U.K.; Fernando, C.A.; Weerasinghe, G.; Pamunuwa, G.K.; Soliman, I.; Ghulamullah, N.; Rajapaksha, S.M.; et al. Synthesis of Silver Nanoparticles Using Green Reducing Agent: Ceylon Olive (*Elaeocarpus serratus*): Characterization and Investigating Their Antimicrobial Properties. *J. Compos. Sci.* **2024**, *8*, 43. [[CrossRef](#)]
58. Choi, O.; Deng, K.K.; Kim, N.J.; Ross, L., Jr.; Surampalli, R.Y.; Hu, Z. The inhibitory effects of silver nanoparticles, silver ions, and silver chloride colloids on microbial growth. *Water Res.* **2008**, *42*, 3066–3074. [[CrossRef](#)] [[PubMed](#)]
59. Hamida, R.S.; Ali, M.A.; Goda, D.A.; Khalil, M.I.; Al-Zaban, M.I. Novel biogenic silver nanoparticle-induced reactive oxygen species inhibit the biofilm formation and virulence activities of Methicillin-Resistant *Staphylococcus aureus* (MRSA) strain. *Front. Bioeng. Biotechnol.* **2020**, *8*, 433. [[CrossRef](#)] [[PubMed](#)]
60. Sondi, I.; Salopek-Sondi, B. Silver nanoparticles as antimicrobial agent: A case study on *E. coli* as a model for Gram-negative bacteria. *J. Colloid Interface Sci.* **2004**, *275*, 177–182. [[CrossRef](#)]
61. Ahmed, S.; Ahmad, M.; Swami, B.L.; Ikram, S. A review on plants extract mediated synthesis of silver nanoparticles for antimicrobial applications: A green expertise. *J. Adv. Res.* **2016**, *7*, 17–28. [[CrossRef](#)]
62. Zhang, X.F.; Liu, Z.G.; Shen, W.; Gurunathan, S. Silver nanoparticles: Synthesis, characterization, properties, applications, and therapeutic approaches. *Int. J. Mol. Sci.* **2016**, *17*, 1534. [[CrossRef](#)]
63. Chaloupka, K.; Malam, Y.; Seifalian, A.M. Nanosilver as a new generation of nanoproduct in biomedical applications. *Trends Biotechnol.* **2010**, *28*, 580–588. [[CrossRef](#)]
64. Neira, L.F.; Vera, A.M.; Escobar, P. Genotoxicidad del nifurtimox en diferentes líneas celulares utilizando el ensayo cometa. *Rev. Médica Risaralda* **2016**, *22*, 3–8. [[CrossRef](#)]

Disclaimer/Publisher’s Note: The statements, opinions and data contained in all publications are solely those of the individual author(s) and contributor(s) and not of MDPI and/or the editor(s). MDPI and/or the editor(s) disclaim responsibility for any injury to people or property resulting from any ideas, methods, instructions or products referred to in the content.